# Unraveling Conformer Specific Sources of Hydroxyl Radical Production from an Isoprene-Derived Criegee Intermediate by Deuteration

Anne S. Hansen, Ziao Liu, Shuguang Chen, Mac G. Schumer, Patrick J. Walsh, and Marsha I. Lester\*

Department of Chemistry, University of Pennsylvania Philadelphia, PA 19104-6323

## Abstract

Ozonolysis of isoprene, the most abundant volatile organic compounds emitted into the Earth's troposphere after methane, yields three distinct Criegee intermediates. Among these, methyl vinyl ketone oxide (MVK-oxide) is predicted to be the major source of atmospheric hydroxyl radicals (OH) from isoprene ozonolysis. Previously, Barber et al. [J. Am. Chem. Soc. 140, 10866-10880 (2018)] demonstrated that syn-MVK-oxide conformers undergo unimolecular decay via 1,4hydrogen (H) transfer from the methyl group to the adjacent terminal oxygen atom, followed by prompt release of OH radical products. Here, we selectively deuterate the methyl group of MVKoxide ( $d_3$ -MVK-oxide) and record its IR action spectrum in the vinyl CH stretch overtone ( $2v_{\text{CH}}$ ) region. The resultant time-dependent appearance of OD radical products, detected by laserinduced fluorescence, demonstrates that unimolecular decay of  $d_3$ -MVK-oxide proceeds by an analogous 1,4-deuterium (D) atom transfer mechanism anticipated for syn-conformers. The experimental spectral and temporal results are compared with the calculated IR absorption spectrum and unimolecular decay rates predicted by Rice–Ramsperger–Kassel–Marcus (RRKM) theory for  $syn-d_3$ -MVK-oxide, as well as the prior study on syn-MVK-oxide. The  $d_3$ -MVK-oxide IR action spectrum is similar to that for MVK-oxide, yet exhibits notable changes as the overtone and combination transitions involving CD stretch shift to lower frequency. The unimolecular decay rate for  $d_3$ -MVK-oxide is predicted to be a factor of 40 times slower than MVK-oxide in the 2v<sub>CH</sub> region. Experimentally, the temporal profile of the OD products reflects the slower unimolecular decay of  $d_3$ -MVK-oxide compared to that for MVK-oxide to OH products as well as experimental factors. Both experiment and theory demonstrate that quantum mechanical tunneling plays a very important role in the 1,4-H/D transfer processes at energies in the vicinity of the transition state barrier. The similarities of the IR action spectra and changes in the unimolecular decay dynamics upon deuteration indicate that syn conformers make the main contribution to the IR action spectra of MVK-oxide and  $d_3$ -MVK-oxide.

1

<sup>\*</sup> Corresponding author email: milester@sas.upenn.edu

### 1. Introduction

The hydroxyl (OH) radical is the most important oxidant in the troposphere. 1,2 It controls the atmospheric lifetime of most trace gases in the troposphere and directly impacts the abundance of greenhouse gases and pollutants in the Earth's atmosphere. Upon reaction with volatile organic compounds, OH typically abstracts a hydrogen atom from organic pollutants initiating reactions that eventually lead to water-soluble products, which can be removed from the troposphere via rain and snow. The concentrations and sources of the OH radical are therefore highly important, especially for accurate modeling of atmospheric chemistry. Alkene ozonolysis is a significant non-photolytic route to the OH radical during day- and night-time.<sup>3, 4</sup> Alkene ozonolysis occurs by cycloaddition of ozone (O<sub>3</sub>) across the alkene double bond (C=C) forming a primary ozonide (POZ) species, which rapidly decomposes to an energized carbonyl oxide (Criegee intermediate) and carbonyl (aldehyde or ketone) species.<sup>1</sup> The Criegee intermediate is produced with internal excitation and may decay promptly to the OH radical and other products.<sup>1,5-8</sup> Alternatively, the energized Criegee intermediate can be collisionally stabilized prior to thermal decay, again producing the OH radical and other products.<sup>5-7, 9-13</sup> As shown in Scheme 1, unimolecular decay to OH radical products generally proceeds by 1,4-hydrogen (H) atom transfer from an alkyl group adjacent to the terminal oxygen of the Criegee intermediate, leading to a vinyl hydroperoxide (VHP) species. VHP undergoes prompt O-O bond cleavage and dissociation to OH and vinoxy radicals.<sup>6, 14-16</sup> The H-transfer process leading to OH radical products occurs for Criegee intermediates with an α-alkyl H-atom syn to the carbonyl oxide group, such as syn-CH<sub>3</sub>CHOO and (CH<sub>3</sub>)<sub>2</sub>COO.<sup>7, 11-13, 17, 18</sup>

Scheme 1: General 1,4 H-atom transfer mechanism for the unimolecular decay of Criegee intermediates with a syn-alkyl  $\alpha$  H-atom.

Alternative unimolecular decay pathways<sup>10</sup> and bimolecular reactions (with  $H_2O$ ,  $SO_2$ ,  $NO_2$  and acids)<sup>8, 19-32</sup> may also be important, and are strongly dependent on the substituents and conformation of the Criegee intermediates. For example, reaction with water vapor (monomer and

dimer) is the dominant removal pathway in the atmosphere for CH<sub>2</sub>OO and *anti*-CH<sub>3</sub>CHOO, which lack an  $\alpha$ -alkyl H-atom *syn* to the carbonyl oxide group. <sup>21, 23, 24</sup>

Isoprene (2-methyl-1,3-butadiene) is the most abundant volatile organic compound emitted into the Earth's troposphere after methane.<sup>1,2</sup> The predominant atmospheric removal pathways for isoprene are reaction with OH, O<sub>3</sub>, and NO<sub>3</sub>. Globally, ozonolysis removes ~10% of isoprene<sup>33</sup> and is an important pathway to OH radicals. Experimental studies of isoprene ozonolysis estimate the yield of the OH radical to be in the range of 20 – 70%, with an IUPAC recommended yield of 25%.<sup>9,34-36</sup> Isoprene has two distinct double bonds and can produce two different POZs.<sup>33,34,37-39</sup> One decomposition channel of POZ can result in methyl vinyl ketone oxide ((CH<sub>2</sub>=CH)(CH<sub>3</sub>)COO, MVK-oxide, ca. 23%, Scheme 2 and Figure 1) + formaldehyde (CH<sub>2</sub>O) or formaldehyde oxide (CH<sub>2</sub>OO) + methyl vinyl ketone ((CH<sub>2</sub>=CH)(CH<sub>3</sub>)CO, MVK), whereas another channel can produce CH<sub>2</sub>OO + methacrolein ((CH<sub>2</sub>=C(CH<sub>3</sub>))CHO, MACR) or methacrolein oxide ((CH<sub>2</sub>=C(CH<sub>3</sub>))CHOO, MACR-oxide, ca. 19%) + formaldehyde.<sup>33</sup> MVK-oxide is predicted to be the more abundant of the two four-carbon unsaturated Criegee intermediates and the major source of OH radicals from atmospheric isoprene ozonolysis.<sup>33</sup>

Scheme 2: Criegee intermediates and co-products formed in ozonolysis of isoprene.

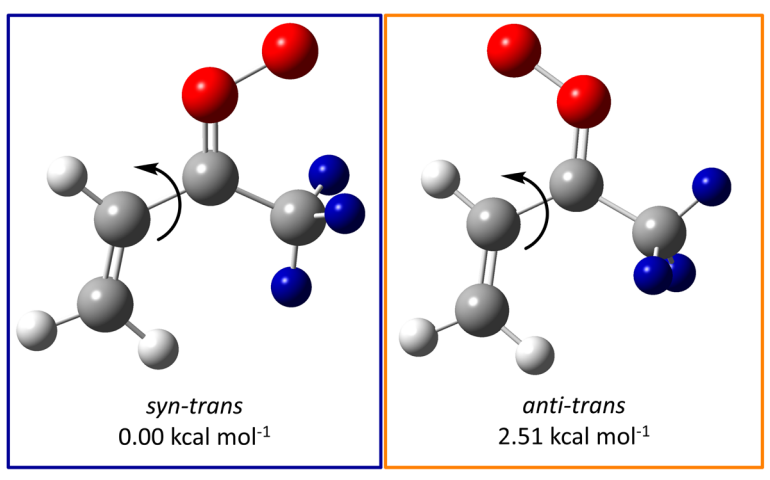


Figure 1: The *syn-trans* and *anti-trans* structures of the methyl vinyl ketone oxide (MVK-oxide) Criegee intermediate. For  $d_3$ -MVK-oxide, the methyl group is deuterated as indicated by the blue coloring. Rotation of the vinyl group (indicated by arrows) produces the corresponding cis conformers. Relative zero-point corrected energies (ANL0-B2F) are also given, see Table S1 for energies of cis conformers.

Direct experimental detection of Criegee intermediates was enabled in 2012<sup>25, 26</sup> by synthesizing gem-diiodoalkane precursors that are either photolyzed or passed through an electric discharge<sup>40-45</sup> to generate a monoiodo alkyl radical, which subsequently reacts with oxygen (O<sub>2</sub>) to form the Criegee intermediate.<sup>25, 26, 42, 46-51</sup> For the four-carbon, unsaturated Criegee intermediates, MVK-oxide<sup>52, 53</sup> and MACR-oxide,<sup>54</sup> allylic monoiodo alkene radicals were photolytically generated from synthesized diiodide precursors. MVK-oxide was first detected in 2018 under jet-cooled conditions by infrared (IR)-action spectroscopy and UV-vis electronic spectroscopy.<sup>52, 53</sup> Additional studies of MVK-oxide have utilized UV-vis transient absorption and photoionization mass spectrometry detection schemes under thermal conditions.<sup>55, 56</sup> MVKoxide has four conformers with similar ground state energies (within 3.1 kcal mol<sup>-1</sup>). Syn and anti conformers shown in Fig. 1 refer to the orientation of the methyl group with respect to the terminal O atom, while the orientation of the vinyl group, cis and trans, differ by rotation about the C-C bond. We anticipate that all four conformers are formed with similar yields and are stabilized under jet-cooled conditions; under thermal conditions the cis and trans conformers are able to interconvert.<sup>55</sup> However, different experimental techniques provide selective detection of specific conformers. IR action spectroscopy under jet-cooled conditions with OH (or OD) detection affords selective detection of those conformers – principally syn conformers – that undergo unimolecular decay to OH (or OD) products.<sup>57</sup>

In the present studies, we focus on IR action spectroscopy and unimolecular decay of selectively deuterated MVK-oxide ( $d_3$ -MVK-oxide). Previously, MVK-oxide was activated with two quanta of CH stretch (2vcH) via IR excitation, providing sufficient energy to surmount or tunnel through the transition state (TS) barrier for the 1,4 H-atom transfer reaction, as illustrated in Scheme 3. Once MVK-oxide undergoes the 1,4 H-atom transfer, 2-hydroperoxybuta-1,3-diene (HPBD) is formed, which undergoes prompt O-O bond cleavage and dissociation to OH and oxybutadiene (((CH<sub>2</sub>=CH)(CH<sub>2</sub>)CO, OBD) radical products. (Note that HPBD and OBD are analogous to VHP and vinoxy formed in the unimolecular decay of syn-CH<sub>3</sub>CHOO.) The experimentally observed rate measurements for appearance of OH products from MVK-oxide was ca.  $2 \times 10^6$  s<sup>-1</sup> (at 6200 cm<sup>-1</sup>), and agreed with statistical unimolecular decay rates (including quantum mechanical tunneling) computed for syn-MVK-oxide.<sup>52</sup> The agreement between experiment and theory also validated the relatively high computed TS barrier of 18.0 kcal mol<sup>-1</sup>, which is  $\sim 1-2$  kcal mol<sup>-1</sup> higher than found for saturated methyl- and ethyl-substituted Criegee intermediates,  $^{12, 17}$  and nearly 2-3 kcal mol<sup>-1</sup> higher than those for the four-carbon saturated methyl-ethyl Criegee intermediate ((CH<sub>3</sub>CH<sub>2</sub>)(CH<sub>3</sub>)COO).<sup>51</sup> The thermal unimolecular decay rate for syn-MVK-oxide was predicted from master equation modeling<sup>52</sup> and confirmed experimentally<sup>55</sup> to be much slower (33 s<sup>-1</sup> at 298 K, 1 atm) than that for saturated Criegee intermediates  $(200 - 600 \text{ s}^{-1} \text{ at } 298 \text{ K}, 1 \text{ atm}).^{51, 52}$ 

Scheme 3: Unimolecular decay pathway for 1,4 H-atom transfer of IR activated *syn-trans*-MVK-oxide leading to OH radical products. A corresponding pathway exists for 1,4 D-atom transfer of  $syn-d_3$ -MVK-oxide indicated by the blue coloring.

The rate for bimolecular reaction of *syn*-MVK-oxide with water vapor (monomer or dimer) has recently been found to be remarkably slow (ca. 1 s<sup>-1</sup>), <sup>10, 55, 58, 59</sup> while MVK-oxide reacts rapidly with formic acid and SO<sub>2</sub>. <sup>55</sup> Global modeling indicates that the reactions of *syn*-MVK-oxide with formic acid and SO<sub>2</sub> are atmospherically important processes in terms of loss of formic acid and production of SO<sub>3</sub> and sulfuric acid. <sup>55</sup> Under atmospheric conditions, thermal unimolecular decay of *syn*-MVK-oxide *via* 1,4 H-atom transfer is expected to be the primary loss process and the major

source of OH radical products from isoprene ozonolysis.<sup>33</sup>

By selectively deuterating the methyl group of MVK-oxide to generate  $syn-d_3$ -MVK-oxide, the 1,4-deuterium (D) atom transfer process is expected to release OD radical products exclusively. In this study, we report the IR action spectrum of  $syn-d_3$ -MVK-oxide in the  $2v_{CH}$  region with detection of OD radical products. Additionally, we present experimental measurements of the temporal profile for appearance of OD products. The experimental results are compared with calculated IR absorption spectra and Rice-Ramsperger-Kassel-Marcus (RRKM) statistical unimolecular decay rates. Comparison with previous results obtained for MVK-oxide gives insight into tunneling effects and illustrates that the 1,4 H/D-atom mechanism is the primary unimolecular decay pathway for syn-MVK-oxide and syn- $d_3$ -MVK-oxide.

### 2. Methods

## 2.1. Experimental

 $d_3$ -MVK-oxide is formed from the photolysis of the (Z/E)-1,3-diiodobut-2-ene-4,4,4- $d_3$  precursor and subsequent reaction with  $O_2$ . The synthesis of the precursor is similar to that of (Z/E)-1,3-diiodobut-2-ene,<sup>52</sup> with specific changes to the synthetic procedure and analytical characterization are provided in Supporting Information (SI, Figures S1 – S6 and Scheme S1). The pulsed jet source has been described in detail previously for other Criegee intermediates.<sup>46, 47, 50, 51</sup> In brief, the heated (65 °C) precursor is seeded in a 20%  $O_2$ /Ar carrier gas (30 psig) and pulsed through the valve and an affixed quartz capillary reactor tube (~25 mm length and 1 mm ID) into a vacuum chamber. The precursor is photolyzed at the tip of the capillary using the 248 nm output of a KrF excimer laser (cylindrically focused, ca. 26 mJ/pulse, Coherent COMPex Pro 50F, 20 Hz) to produce an allylic monoiodoalkene radical that subsequently reacts with  $O_2$  to form  $d_3$ -MVK-oxide (see Scheme S2).  $d_3$ -MVK-oxide is collisionally stabilized and thermalized in the capillary, and cooled in the supersonic jet expansion.

 $d_3$ -MVK-oxide is initially detected by photoionization using 10.5 eV (118 nm) vacuum ultraviolet (VUV) radiation on the parent m/z = 89 mass channel of a time-of-flight mass spectrometer (TOF-MS, RM Jordan) as described previously for other Criegee intermediates.  $^{46, 47, 50, 53}$  The present study focuses on IR action spectroscopy of the  $d_3$ -MVK-oxide Criegee intermediates. IR excitation in the  $2v_{CH}$  region excites stabilized  $d_3$ -MVK-oxide and initiates unimolecular decay. The resultant OD radical products are detected by UV laser-induced

fluorescence (LIF). Approximately 1 cm downstream (collision-free region) from the tip of the capillary, overlapping IR-pump (focused to ca. 3 mm diameter) and UV-probe (focused to ca. 5 mm diameter) beams intersect with the gas mixture containing stabilized  $d_3$ -MVK-oxide. The IR-pump is the signal output of a LaserVision KTP-based OPO that is pumped by a Continuum Surelite EX Nd:YAG laser (10 Hz). The UV-probe is the frequency doubled output of a Nd:YAG pumped dye laser (20 Hz). Other experimental methods are analogous to the previous study on MVK-oxide and are provided in the SI. An active background subtraction scheme (IR on –IR off) is used to remove background OD signal, which arises from the unimolecular decay of energized  $d_3$ -MVK-oxide in the capillary and subsequent cooling in the free jet expansion.

## 2.2. Computational

Electronic structure calculations of the Criegee intermediates, relevant TS barriers, and products are performed in Gaussian16 at the B2PLYP-D3/cc-pVTZ level of theory.<sup>60-62</sup> We utilize structures (MVK-oxide, TS, and products) previously optimized in Gaussian09 and electronic energies calculated at the ANL0-B2F level of theory (CCSD(T)-F12/CBS-F12(TZ-F12,QZ-F12)//B2PLYP-D3/cc-pVTZ) in Molpro.<sup>52</sup> The IR absorption spectrum of *d*<sub>3</sub>-MVK-oxide in the 2v<sub>CH</sub> region is calculated (B2PLYP-D3/cc-pVTZ) using vibrational second order perturbation theory (VPT2) as implemented in Gaussian16. Calculations were performed utilizing XSEDE resources.<sup>63</sup>

The energy-dependent unimolecular decay rate, k(E), for  $d_3$ -MVK-oxide is calculated using statistical RRKM theory. Quantum mechanical tunneling is included using semiclassical transition state theory (SCTST) as implemented in Multiwell 2019. The RRKM calculations are analogous to those carried out previously. In the present study, the anharmonic fundamental vibrational frequencies as well as the anharmonicity matrix of the reactants and TS, used as input parameters in Multiwell, are calculated at the B2PLYP-D3/cc-pVTZ (Gaussian16) level of theory. The potential energy surface for the methyl and vinyl torsions, obtained from ref. 52, are calculated at the B2PLYP-D3/cc-pVTZ (Gaussian09) level of theory. For consistency, we also recalculate the unimolecular decay rate for MVK-oxide with Multiwell 2019 using frequencies calculated in Gaussian 16; see SI for details.

#### 3. Results

In this study, we investigate  $d_3$ -MVK-oxide to elucidate the mechanism for formation of the OD radical product.  $d_3$ -MVK-oxide exhibits the same four distinct conformers as MVK-oxide within two classes, syn and anti, which differ in the orientation of the deuterated methyl group with respect to the terminal oxygen of the carbonyl oxide group (Figure 1). The energy barrier between these two classes is high (ca. 30 kcal mol<sup>-1</sup>),  $^{10, 38, 52}$  and thus syn- and anti-conformers are taken to be distinct species that do not interconvert. The interconversion barrier between trans and cis is low (ca. 8 kcal mol<sup>-1</sup>),  $^{52}$  and we anticipate that trans- and cis-conformers will readily interconvert upon IR activation at the energies, ca. 17 kcal mol<sup>-1</sup> (5750 – 6260 cm<sup>-1</sup>), used in this work.

We record the IR action spectrum of  $d_3$ -MVK-oxide (5900 – 6250 cm<sup>-1</sup>) by scanning the OPO with LIF detection of the OD radical products on the  $A^2\Sigma - X^2\Pi_{3/2}$  (1,0)  $Q_1(3)$  transition at a fixed IR-UV time delay. The IR action spectrum is compared to the calculated IR absorption spectra of the  $d_3$ -MVK-oxide conformers. We also compare the IR action spectrum of  $d_3$ -MVK-oxide (OD LIF) with that previously reported for MVK-oxide (OH LIF).<sup>52</sup> The OD product appearance rate is investigated theoretically (RRKM theory) and experimentally. In these experiments, the IR frequency is fixed on specific IR transitions of  $d_3$ -MVK-oxide, while the IR-UV time delay is varied.

## 3.1 IR Spectroscopy

## 3.1.1 Computed IR absorption spectrum

Both the *syn*- and *anti-d*<sub>3</sub>-MVK-oxide conformers have IR transitions in the  $2v_{CH}$  region (Figure S9). The *syn-d*<sub>3</sub>-MVK-oxide conformers are predicted to produce OD radical products *via* a 1,4 D-atom transfer mechanism (Scheme 3), while the *anti* conformers are not expected to contribute to the formation of OD radical products, which will be discussed in Section 4.3. As a consequence, only IR transitions calculated for the *syn* conformers are presented herein and compared to the observed IR action spectrum. As shown in Figure 2, the strongest IR transitions for the *syn-trans* and *syn-cis* conformers of *d*<sub>3</sub>-MVK-oxide are predicted at ~6200 cm<sup>-1</sup> and arise from the out-of-phase vinyl CH stretch overtone transitions (2v<sub>1</sub>). The weak adjacent transitions at ~6180 cm<sup>-1</sup> are out-of-phase vinyl and methine CH stretch combination bands (v<sub>1</sub>+v<sub>2</sub>). The cluster of transitions predicted at 6000 to 6100 cm<sup>-1</sup> are additional overtone CH stretching

vibrations and combination bands associated with vinyl  $(v_1, v_3)$  and methine  $(v_2)$  groups (see Table S2).

The computed IR intensities reflect the intrinsic strength of the IR transitions and assume equal population of the two *syn* conformers. Up to two quanta changes are considered in the computed IR absorption spectra (VPT2); higher order excitations are not included. The computed spectra shown in Figure 2 are obtained by convoluting the stick spectra (Figure S9) with a Gaussian function (FWHM of  $\sim$ 4.7 cm<sup>-1</sup>) that reflects the typical breadth of a rotational band contour under the jet-cooled experimental conditions (10 K). <sup>15, 16</sup> The breadth is determined by simulation of the 6202 cm<sup>-1</sup> feature of *syn-trans-d*<sub>3</sub>-MVK-oxide (see Figure S10). The computed IR transitions predicted for the two *syn* conformers are also combined (Figure 2, grey trace), since the two conformers readily interconvert upon IR excitation.

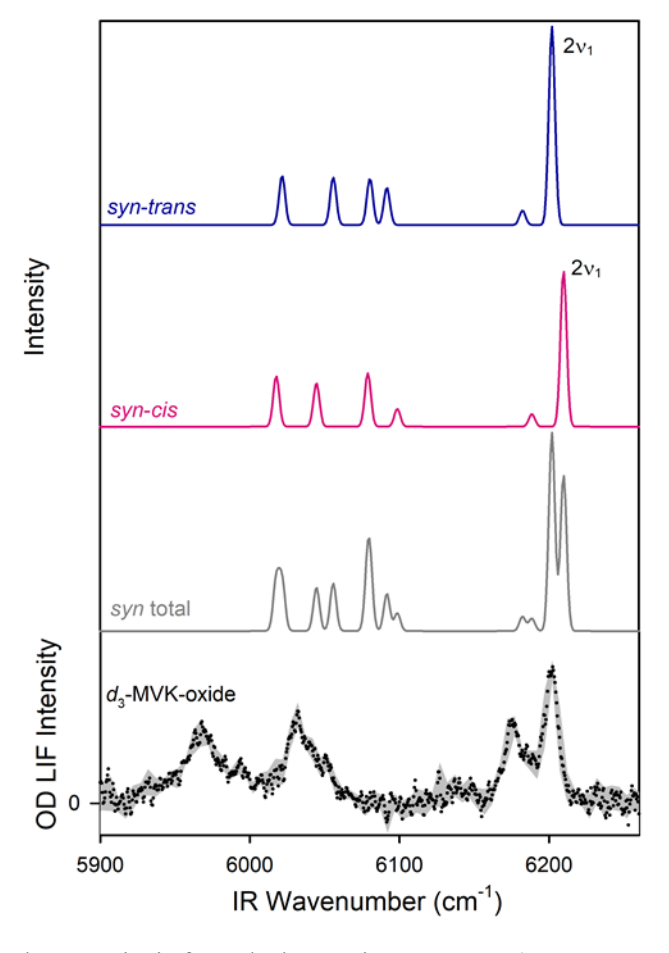


Figure 2: Calculated anharmonic infrared absorption spectra (B2PLYP-D3/cc-pVTZ) in the CH stretch overtone region for the two syn conformers of  $d_3$ -MVK-oxide; see text for detail. The experimental IR action spectrum is obtained with OD LIF detection at a fixed IR-UV time delay

of 2000 ns. Black points represent experimental data, while the grey shaded area represents a smoothed version including  $\pm 1\sigma$ .

## 3.1.2 Experimental IR action spectrum

The experimental IR action spectrum of  $d_3$ -MVK-oxide is recorded in the  $2v_{CH}$  region with UV LIF detection of OD radical products on the A-X (1,0) Q<sub>1</sub>(3) transition at a fixed IR-UV time delay of 2000 ns and a scan speed of 0.05 cm<sup>-1</sup>/s. The experimental spectrum from 5900 to 6250 cm<sup>-1</sup> is shown in Figure 2 and is an average of several scans (black points). The grey shaded area represents one standard deviation ( $\pm 1\sigma$ ) about a smoothed version of the data. The IR-UV time delay is selected based on preliminary measurements of the OD appearance rate to obtain maximum LIF signal. The fact that the optimum IR-UV time delay is 2000 ns for acquiring the IR action spectrum indicates that the 1,4 D-transfer process is slow compared to the H-transfer process investigated previously for MVK-oxide.<sup>52</sup> It is also a much longer time delay than required for the H-atom transfer process in other alkyl substituted Criegee intermediates as well as the Dtransfer process in syn-CD<sub>3</sub>CHOO. <sup>12, 13, 17, 57</sup> An IR action spectrum (6160 – 6220 cm<sup>-1</sup>) with a time delay of 800 ns was also recorded (Figure S11). Overall, the intensity of the observed features decreased equally and no additional features appeared. The experimental spectrum exhibits four distinctive features peaked at 6202, 6175, 6030, and 5960 cm<sup>-1</sup>. The two higher wavenumber features are partially overlapped; the two lower wavenumber features have noticeably greater breadth. All four features are broader than anticipated for isolated features with a rotational band contour at 10 K. An overlay of the IR action spectrum (6160 – 6215 cm<sup>-1</sup>) and the simulated band contours of the 6175 cm<sup>-1</sup> and 6202 cm<sup>-1</sup> features (Figure S12) illustrates that additional homogeneous broadening beyond that previously determined for CH<sub>3</sub>CHOO (1.7 cm<sup>-1</sup>)<sup>16</sup> and  $(CH_3)_2COO(2.1 \text{ cm}^{-1})^{15}$  is likely present for  $d_3$ -MVK-oxide.

Overall, the observed IR action spectrum in the  $2v_{CH}$  region is reasonably well represented by the calculated IR absorption spectrum of  $syn-d_3$ -MVK-oxide. Based on the calculated frequencies, we attribute the strong experimental features at 6202 and 6175 cm<sup>-1</sup> to the out-of-phase vinyl CH stretch overtone transitions ( $2v_1$ ) of the syn-cis and syn-trans conformers, respectively. The features centered at 6030 and 5960 cm<sup>-1</sup> likely arise from the cluster of transitions predicted between 6000 to 6100 cm<sup>-1</sup> for both syn-cis and syn-trans conformers involving CH stretch overtones and combination bands of the vinyl and methine groups. The congestion observed in the experimental spectrum is attributed to overlapping transitions and

spectral broadening arising from intramolecular vibrational redistribution (IVR), as discussed in Section 4.1.

Following IR excitation of  $d_3$ -MVK-oxide at 6202 cm<sup>-1</sup>, the UV probe wavelength is also varied to measure the product state distribution of the resulting OD  $X^2\Pi_{3/2}$  (v=0) radicals, as shown in Figure S13. The  $\Pi(A'')$   $\lambda$ -doublet (Q<sub>1</sub>) is favored over the  $\Pi(A')$  level (P<sub>1</sub>) and low rotational levels (N = 2 – 5) of v=0 are most populated, as found for other Criegee intermediates detected under equivalent experimental conditions. <sup>15, 16, 18</sup>

Figure 3 compares the IR action spectrum of  $d_3$ -MVK-oxide observed utilizing OD LIF detection with that previously obtained for MVK-oxide using OH LIF detection in the  $2v_{CH}$  region from 5750 cm<sup>-1</sup> to 6260 cm<sup>-1</sup>.<sup>52</sup> The spectral span extends to lower wavenumber than shown in Figure 2 to include CH stretch overtones and combination bands involving the methyl group of MVK-oxide (Table S3). The overtone transitions and combination bands associated with CD stretches of the deuterated methyl group in  $d_3$ -MVK-oxide are shifted to considerably lower frequency (ca. 4500 cm<sup>-1</sup>) and are not investigated in this study.

Overall, the IR action spectrum for  $d_3$ -MVK-oxide is similar to that for MVK-oxide. In both spectra, the most distinctive features are observed at ~6200 cm<sup>-1</sup>, which arise from out-of-phase vinyl CH stretch overtone transitions (2v<sub>1</sub>) for the *syn-cis* and *syn-trans* conformers. For both  $d_3$ -MVK-oxide and MVK-oxide, overtones and combination bands involving CH stretches of the vinyl and methine groups are predicted from 6000 to 6100 cm<sup>-1</sup> (Tables S2 – S3). For MVK-oxide only, overtones and combination bands involving the CH stretches of the methyl group give rise to additional transitions between 5750 cm<sup>-1</sup> and 6050 cm<sup>-1</sup> (Table S3). These methyl CH transitions add breadth and congestion to the two broad features observed in the MVK-oxide spectrum from 5950 cm<sup>-1</sup> to 6050 cm<sup>-1</sup> compared to that observed for  $d_3$ -MVK-oxide. The methyl CH overtone stretches also appear as weak features in the MVK-oxide spectrum below 5950 cm<sup>-1</sup>. The CH overtone stretches of the methyl group are predicted to be at least 3 to 4 times weaker than the strongest 2v<sub>1</sub> transition (Table S3).

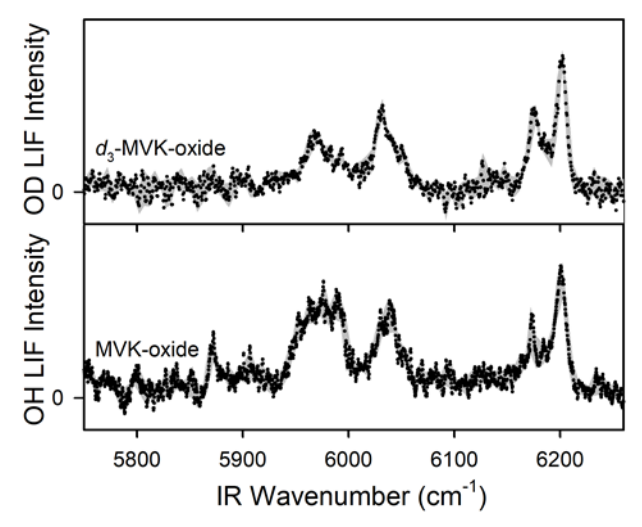


Figure 3: Experimental IR action spectra of  $d_3$ -MVK-oxide with OD LIF detection (2000 ns time delay) and MVK-oxide with OH LIF detection (800 ns time delay).<sup>52</sup> The MVK-oxide data is reproduced with permission from *J. Am. Chem. Soc.* **2018**, *140*, 10866-10880, Copyright © 2018, American Chemical Society. Black points represent experimental data, while the grey shaded area represents a smoothed version including  $\pm 1\sigma$ .

## 3.1.3 Unimolecular decay of $d_3$ -MVK-oxide via 1,4 D-atom transfer

Figure 4 shows the predicted microcanonical RRKM decay rates (and associated lifetimes) for *syn-d*<sub>3</sub>-MVK-oxide conformers with 5750 – 6300 cm<sup>-1</sup> of energy; see also Table S4. A 1,4 D-atom transfer is assumed to be the rate-limiting step for unimolecular decay to OD radical products. In the RRKM calculations complete IVR is assumed. This means that IVR occurs on a much faster timescale (ps) than the OD appearance rate (μs), and that at a given energy all vibrational states are accessible. In Figure 4, we also show the corresponding RRKM rates for the H-atom transfer for *syn*-MVK-oxide conformers that yield OH radical products.<sup>52</sup> These calculations are based on previous high-level electronic structure calculations of the TS barrier for *syn*-MVK-oxide,<sup>52</sup> and changes in the anharmonic frequencies and ZPE of the Criegee intermediate reactant and transition state upon deuteration.

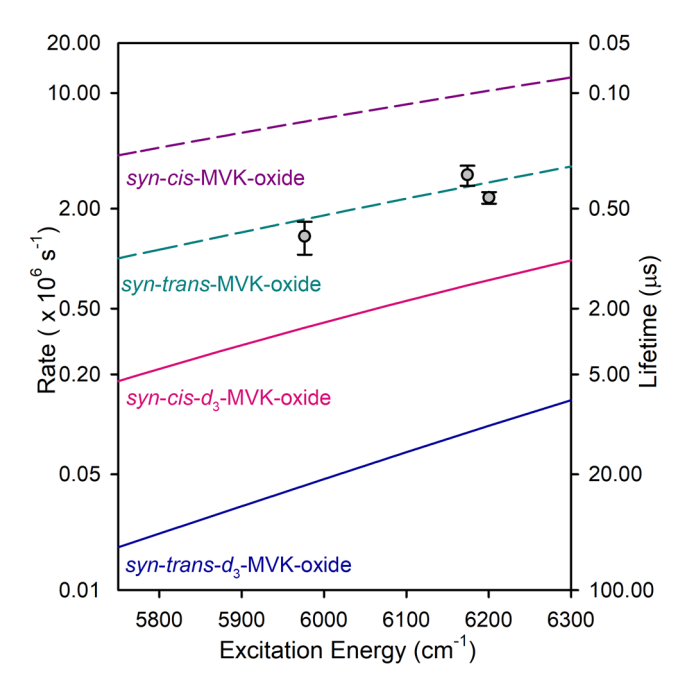


Figure 4: Calculated RRKM rates and lifetimes (semi-log scale) for unimolecular decay *via* 1,4 D-atom transfer for *syn-trans-d*<sub>3</sub>-MVK-oxide (solid blue line) and *syn-cis-d*<sub>3</sub>-MVK-oxide (solid pink line). RRKM rates computed for unimolecular decay *via* 1,4 H-atom transfer for the *syn-trans*-MVK-oxide (dashed cyan line) and *syn-cis*-MVK-oxide (dashed purple line) are also shown, which are updated based on Gaussian 16 anharmonic frequencies.<sup>52</sup> Rates are computed using RRKM theory and including quantum mechanical tunneling (SCTST). Experimental rates (grey circles with error bars) for IR activated *syn*-MVK-oxide are reproduced from *J. Am. Chem. Soc.* **2018**, *140*, 10866-10880, Copyright © 2018, American Chemical Society.

For *syn-trans*-MVK-oxide, the TS barrier is 17.97 kcal mol<sup>-1</sup> (6285 cm<sup>-1</sup>) and the imaginary frequency is 1630*i* cm<sup>-1</sup>.<sup>52</sup> Upon deuteration of the methyl group, the TS barrier increases by 4% to 18.72 kcal mol<sup>-1</sup> (6547 cm<sup>-1</sup>) and the imaginary frequency associated with 1,4 D-atom transfer decreases by 25% to 1198*i* cm<sup>-1</sup> (Table S5). Figure 5 shows the calculated Eckart potentials plotted in mass-weighted coordinates for the reaction of *syn-trans-d*<sub>3</sub>-MVK-oxide (blue) and *syn-trans-MVK*-oxide (cyan) to HPBD *via* 1,4 D- or H-atom transfer. The increase of the TS barrier arising from changes in ZPE of reactant and TS, and decrease of the imaginary frequency (an effective change in the breadth of the barrier) upon deuteration are clearly illustrated in Figure 5.

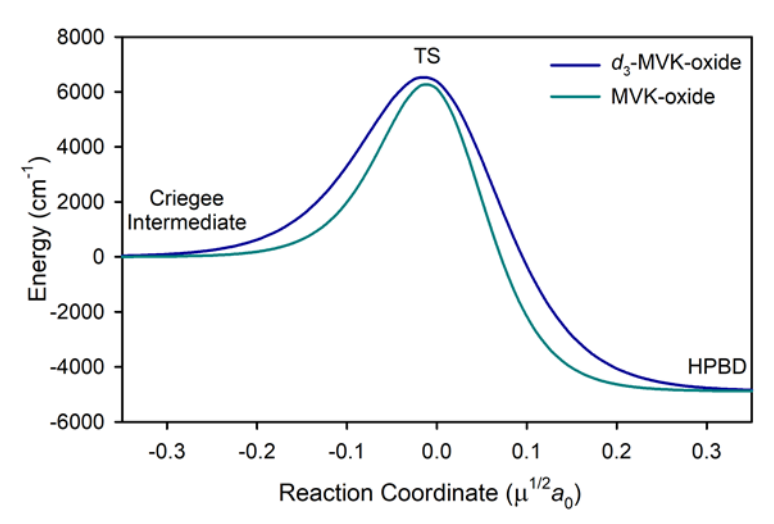


Figure 5: Calculated Eckart potentials plotted in mass-weighted coordinates (reduced mass  $\mu$  and distance  $a_0$ ) for the reaction of *syn-trans-d*<sub>3</sub>-MVK-oxide (blue) and *syn-trans*-MVK-oxide (cyan) to HPBD *via* 1,4 D/H-atom transfer.

At 6000 cm<sup>-1</sup>, the RRKM rates computed for *syn-trans-d*<sub>3</sub>-MVK-oxide ( $k(E) = 4.69 \times 10^4$  s<sup>-1</sup>,  $\tau = 22 \,\mu s$ ) are a factor of 40 slower than those for *syn-trans*-MVK-oxide ( $k(E) = 1.82 \times 10^6 \, s^{-1}$ ,  $\tau = 0.5 \,\mu s$ ). The significant slowing of the unimolecular rates upon deuteration illustrates the importance of tunneling in the 1,4 H/D-atom transfer process associated with unimolecular decay of *syn* conformers. The same effect was previously observed experimentally and confirmed theoretically upon deuteration of the methyl group of *syn*-CH<sub>3</sub>CHOO (*syn*-CD<sub>3</sub>CHOO), where the rate decreased by a factor of 10 at 6055 cm<sup>-1</sup>.<sup>57</sup> For both *syn-d*<sub>3</sub>-MVK-oxide and *syn*-MVK-oxide, the rate for unimolecular decay of the *syn-cis* conformer at a given excitation energy is faster than that for the *syn-trans* conformer. This effect is more pronounced for  $d_3$ -MVK-oxide than for MVK-oxide (Table S4) and may influence the intensity contribution from the individual conformers in the calculated part of Figure 2, as illustrated and discussed in Section 4.2.

The OD temporal profile is also investigated experimentally at specific IR excitation energies. In Figure 6, we show the OD product temporal profile for  $d_3$ -MVK-oxide excited at 6202 cm<sup>-1</sup>. For comparison, also shown is the time profile for OH products from MVK-oxide excited at 6200 cm<sup>-1</sup>.<sup>52</sup> The experimental temporal profile for OD products from  $d_3$ -MVK-oxide reaches its maximum at a much later time (~1400 ns) than that seen for OH products from MVK-oxide (~600 ns). Importantly, experimental factors, which originate from molecules moving out of the UV probe laser region, <sup>11, 17, 52, 57</sup> also affects the observed temporal profile. This purely experimental limitation occurs on a 1 – 2  $\mu$ s time scale under the present conditions. <sup>11, 18, 52, 57</sup> This

experimental constraint precludes direct determination of the rate of appearance of OD products (predicted to be on the order of 20  $\mu$ s) and limits the maximum amplitude of the OD signal that is detected. The slow temporal appearance upon deuteration is predicted theoretically (Figure S14) and observed experimentally at several IR excitation energies (Figure S15). This indicates that OD radical products are formed from the 1,4 D-atom transfer. Even slower unimolecular decay rates are anticipated following IR excitation of  $d_3$ -MVK-oxide at lower energies, again preventing direct experimental determination of the rate. Thus, Figure 6 demonstrates that the unimolecular decay rate of  $d_3$ -MVK-oxide to OD products occurs on a  $\mu$ s or slower timescale and is significantly slower than that for MVK-oxide to OH products, thereby confirming the very important role of quantum mechanical tunneling in the rate-limiting 1,4 H/D-atom transfer process for *syn* conformers that release OH/OD radical products.

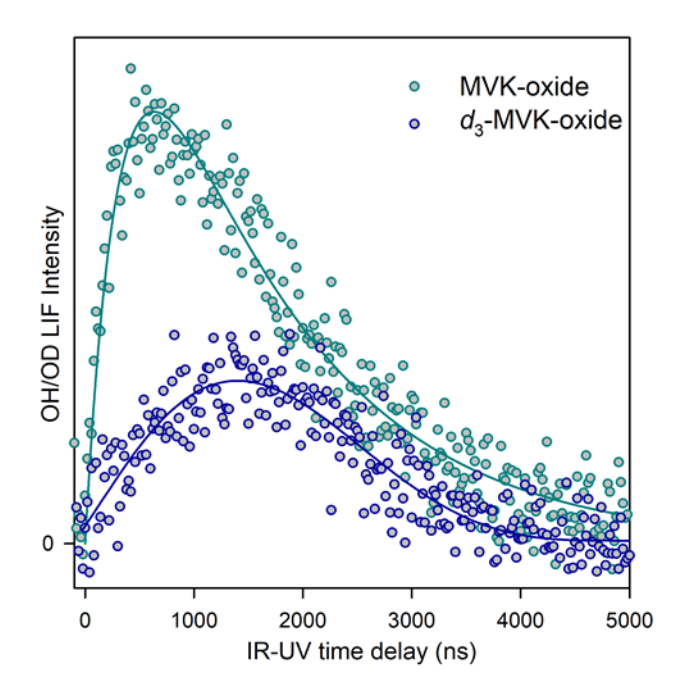


Figure 6: Experimental OH/OD time profiles observed following excitation of the strongest feature in the IR action spectra of MVK-oxide (cyan,  $6200 \text{ cm}^{-1}$ )<sup>52</sup> and  $d_3$ -MVK-oxide (blue,  $6202 \text{ cm}^{-1}$ ). The MVK-oxide data is reproduced with permission from *J. Am. Chem. Soc.* **2018**, *140*, 10866-10880, Copyright © 2018, American Chemical Society. Time profiles are taken in 20 ns increments. For MVK-oxide, the time trace is fitted with a biexponential function (solid line). For  $d_3$ -MVK-oxide, a seventh-order polynomial (solid line) is used to depict the time profile.

The OD signal shown in Figure 2 arises from OD radical products formed from IR activated  $d_3$ -MVK-oxide under collision-free conditions. Analogous IR spectral scans of  $d_3$ -MVK-oxide with OH LIF detection revealed no discernable IR-induced signal. In both cases, OD or OH LIF

background is removed from the IR action spectral scans by active background subtraction (IR on – IR off). In addition, 'background' hydroxyl radicals are formed from unimolecular decay of  $d_3$ -MVK-oxide within the capillary, and are subsequently cooled in the free jet expansion. Surprisingly, both OD and OH radicals are observed as 'background' signals (IR off) following generation of  $d_3$ -MVK-oxide in the capillary. The OD background signal measured by probing the OD  $A^2\Sigma - X^2\Pi_{3/2}$  (1,0)  $Q_1$ (1) transition *via* saturated LIF are larger (by a factor of ~6) than the OH background signal on the OH  $A^2\Sigma - X^2\Pi_{3/2}$  (1,0)  $Q_1$ (1) transition. This is also confirmed by measuring OD and OH background signals on their  $P_1$ (1) transitions. Plausible sources of the OD and OH background signals are considered in the SI.

#### 4. Discussion

## 4.1. Origin of experimental breadth and congestion

Overall, the features observed in the experimental IR action spectrum are in reasonably good agreement with those predicted in the calculated IR absorption spectrum of syn-d<sub>3</sub>-MVKoxide as shown in Figure 2. The predicted vinyl CH stretches are within 8 cm<sup>-1</sup> of the observed frequency, while a larger discrepancy (50 cm<sup>-1</sup>) is found between calculated and observed frequencies for the CH stretch combination bands. This discrepancy is probably due to the level of theory (restricted by the molecular size) and the limitations of the theory (only two quanta changes) used. The breadth of the features in the IR action spectrum is larger than theoretically predicted, as found previously.<sup>51</sup> The congestion in the experimental spectrum likely arises from additional homogenous broadening of the rotational band contour and/or higher order coupling between bright and dark states not included in the anharmonic frequency calculations. Homogenous broadening is attributed to rapid IVR (2 - 3 ps), as previously observed for CH<sub>3</sub>CHOO and (CH<sub>3</sub>)<sub>2</sub>COO in the 2v<sub>CH</sub> region. <sup>15, 16</sup> Torsional modes are known to increase the density of states and accelerate IVR.<sup>18</sup> An overlay of the simulated band contours for the 6175 and 6202 cm<sup>-1</sup> features in the IR action spectrum (Figure S12) illustrates that the methyl and vinyl torsional motions of  $d_3$ -MVK-oxide introduce additional homogeneous broadening compared to that previously determined for CH<sub>3</sub>CHOO (1.7 cm<sup>-1</sup>) and (CH<sub>3</sub>)<sub>2</sub>COO (2.1 cm<sup>-1</sup>). <sup>15, 16</sup> Higher order couplings would result in greater breadth of the IR features and increase congestion in the IR action spectrum compared to the simulated spectrum. Higher order couplings could be between zeroorder states that carry significant IR oscillator strength (bright states) and nearby states involving two or more quanta of excitation that lack intrinsic IR oscillator strength (dark states). Dark states involving low frequency torsional modes are known to enhance such coupling.<sup>66</sup> The low-frequency torsional modes for  $d_3$ -MVK-oxide give rise to numerous dark states involving torsion in the  $2v_{CH}$  energy regime. Hence, VPT2 appears to be insufficient for a full spectroscopic description of the larger Criegee intermediates and more sophisticated methods (cubic and quadratic couplings) are needed.

## 4.2. 1,4 D-transfer process – source of OD radical products

The dominant unimolecular removal pathway predicted for  $syn-d_3$ -MVK-oxide conformers is the 1,4 D-atom transfer process that produces OD radical products. IR activation of  $d_3$ -MVK-oxide is found to yield OD radicals, but not OH radicals. The computed RRKM unimolecular decay rate significantly decreases upon deuteration. For example, k(E) for the syn-trans conformer decreases by factor of 40 at 6000 cm<sup>-1</sup> due to a 15-fold decrease in the tunneling-weighted sum of states and a 2.6-fold increase in the density of reactant states. These changes result in a kinetic isotope effect (KIE) of 40 for syn-trans and 15 for syn-cis conformers at 6000 cm<sup>-1</sup>, as shown in Figure S16. The magnitude of the KIE depends on energy and is most important below the TS barrier where tunneling for D-atoms transfer is much less probable than for H-atoms.

At a given energy, the RRKM rate predicted for *syn-cis* is faster than that for *syn-trans* conformers of  $d_3$ -MVK-oxide (Figure 4). The same is predicted for the *syn*-MVK-oxide conformers, although the change in RRKM rate between *syn-cis* and *syn-trans* conformers of MVK-oxide is less pronounced due to their larger imaginary frequency (Table S5). The unimolecular decay of the *syn-trans* and *syn-cis* conformers will mainly occur *via* the lowest TS energy barrier (*syn-trans*-TS). At a given IR excitation energy, the *syn-cis* conformer, which has a higher ground state energy (1.79 kcal mol<sup>-1</sup>), will be excited to a higher rovibrational state than the *syn-trans* conformer (0.0 kcal mol<sup>-1</sup>), resulting in faster unimolecular decay. The different RRKM rates for the *syn-cis* and *syn-trans* conformers may change their relative intensities in IR action spectra (at a specific IR-UV delay time) as shown in Figure S17. This effect is expected to be greater for  $d_3$ -MVK-oxide than MVK-oxide. In addition, the relative abundances of the *syn-trans* and *syn-cis* conformers under the present experimental conditions (assumed equal in Figure 2) would impact their relative intensities in the IR action spectra.

## 4.3. Additional pathways for loss of the $d_3$ -MVK-oxide conformers

In our experiments, both syn and anti conformers of  $d_3$ -MVK-oxide are expected to be formed. Syn conformers undergo unimolecular decay via the 1,4 D-transfer process described above. A series of pathways have been explored theoretically to identify the energetically favorable pathways for unimolecular loss of anti conformers of MVK-oxide. 10, 37, 52, 67, 68 These pathways are assumed to be similar for anti-d<sub>3</sub>-MVK-oxide. The unimolecular loss pathways for anti-MVK-oxide include: anti to syn isomerization, vinyl H-transfer, and ring closure to dioxole (cyc-CH<sub>2</sub>OOC(CH<sub>3</sub>)CH). <sup>10, 37, 52, 67, 68</sup> The *anti* to *syn* isomerization was found to be unlikely based on a computed barrier of 21.4 kcal mol<sup>-1</sup> (no tunneling) that must be overcome, which is not feasible at an IR excitation energy of 6200 cm<sup>-1</sup> (17.7 kcal mol<sup>-1</sup>).<sup>52</sup> The vinyl H-transfer pathway is also unlikely due to its high TS barrier (>20 kcal mol<sup>-1</sup>). 10, 37, 52 Even though tunneling may occur, the RRKM rate for this reaction at an IR excitation energy of 6200 cm<sup>-1</sup> is extremely slow (~10<sup>3</sup> s<sup>-1</sup>).<sup>52</sup> The most probable unimolecular decay pathway for IR activated *anti*-MVK-oxide is rapid electrocyclic ring closure to form a 5-membered cyclic peroxide known as dioxole (TS barrier of ca. 12.0 kcal mol<sup>-1</sup>). <sup>37, 38, 52</sup> Dioxole will be formed with sufficient internal excitation to undergo further unimolecular decay. The O-O bond will cleave to form a diradical, which can rearrange via 1,2 H-transfer to a β-dicarbonyl (Scheme 8 of Ref. 52). The lowest energy path from the β-dicarbonyl is predicted to be barrierless C-C bond fission to acetyl and vinoxy radical products.52

In a previous study, Barber *et al.* considered the possibility of keto-enol tautomerization from the  $\beta$ -dicarbonyl to an enol formed with sufficient internal energy to undergo unimolecular decay to OH products (Scheme 8 of Ref. 52). In this scenario, the methyl group would act as spectator, and thus *anti*-conformers of  $d_3$ -MVK-oxide could also yield OH products. An alternative UV laser assisted photodissociation pathway from the enol to OH was also considered. There are prior reports in the literature of OH radicals generated by exciting the enol tautomer of acetylacetone with pump laser wavelengths of 266 nm, 291 nm, and 282 nm. <sup>67-69</sup> In our experiments, 282 nm radiation is used for OH A-X (1,0) Q<sub>1</sub> (3) LIF detection. For an analogous UV light driven pathway from the enol tautomer, two sequential single-photon processes would need to occur: UV excitation and OH LIF detection. Again, such a pathway from the enol tautomer (with deuterated methyl group as a spectator) would likely yield OH products. <sup>52</sup>

The above mentioned pathways are potential ways that IR activation of anti conformers of

 $d_3$ -MVK-oxide could result in OH radical products. To test this hypothesis, we investigated the possible production of OH radicals following IR activation of  $d_3$ -MVK-oxide. We were unable to detect OH radical product signals while scanning the IR frequency from 6100 - 6250 cm<sup>-1</sup> at various IR-UV time delays. This demonstrates that there is no observable OH radical products produced upon IR activation of stabilized and jet cooled  $d_3$ -MVK-oxide. Thus, there is no direct evidence of keto-enol tautomerization in our experiment. Finally, the similarities between the IR action spectra of MVK-oxide and  $d_3$ -MVK-oxide indicate that syn conformers make the principle contribution to the IR action spectrum of MVK-oxide shown in Figure 3.

In addition to IR-induced excitation of  $d_3$ -MVK-oxide with LIF detection of OD products, some 'background' OH and OD products are observed (IR off) that originate from unimolecular decay of  $d_3$ -MVK-oxide and potential secondary chemistry within the capillary. The 'background' OH and OD products are subsequently cooled in the free jet expansion and their LIF signals are removed from IR action spectra by active background subtraction. The OH background signal is smaller (typically by a factor of 6) than the OD background signal. There are multiple possible sources for OH/OD background signals that we explore in the SI.

## 5. Conclusion

The IR action spectrum of selectively deuterated MVK-oxide,  $d_3$ -MVK-oxide, is obtained in the CH overtone stretch ( $2v_{CH}$ ) region with time-resolved LIF detection of OD radical products. The spectrum is dominated by two strong features around ~6200 cm<sup>-1</sup>, which are ascribed to the first overtone CH stretch associated with the vinyl group of the syn- $d_3$ -MVK-oxide conformers. Additionally, two broad features are observed at lower frequency (6030 cm<sup>-1</sup> and 5960 cm<sup>-1</sup>) that originate from a cluster of transitions involving CH stretch overtones and combination bands of the vinyl and methine groups. The IR action spectrum of  $d_3$ -MVK-oxide (OD detection) and that previously obtained for MVK-oxide (OH detection) are similar. The main differences in the spectra are observed from ca. 5800 - 6100 cm<sup>-1</sup>, where the methyl group of MVK-oxide gives rise to additional CH stretching transitions not present in  $d_3$ -MVK-oxide, which also add breadth and congestion to the features within this region. Selective deuteration affects the IR frequencies and, even more importantly, the 1,4 D/H-atom transfer and associated unimolecular decay rate that gives rise to OD/OH radical products. The 1,4 D-atom transfer process of syn- $d_3$ -MVK-oxide is significantly slower than the H-atom transfer process of syn-MVK-oxide. Deuteration has a large

effect at energies below the TS barrier, where tunneling is important and less probable for D-atoms compared to H-atoms. IR activation of  $d_3$ -MVK-oxide demonstrates that the main source of hydroxyl radicals is from 1,4 D-atom transfer and associated unimolecular decay of syn conformers of  $d_3$ -MVK-oxide.

## Supporting Information Available

Synthesis details and analytical data, additional experimental and theoretical details, computed and experimental IR spectra and time profiles, OD product state distribution, kinetic isotope effect, and tabulation of calculated frequencies, intensities, and RRKM rates.

This material is available free of charge *via* the Internet at http://pubs.acs.org/

## Acknowledgements

This research was primarily supported through the National Science Foundation under grant CHE-1664572 (MIL). This work used the Extreme Science and Engineering Discovery Environment (XSEDE), which is supported by National Science Foundation grant number ACI-1548562 through the allocation TG-CHE190088. ASH gratefully acknowledges support from the Carlsberg Foundation (CF18-0614) and the Independent Research Fund Denmark (9036-00016B). PJW thanks the National Science Foundation (CHE-1902509). Partial support of MGS provided by NIH R35 GM131902 (M. C. Kozlowski, PI). The authors thank Victoria P. Barber (MIT), Shubhrangshu Pandit (UCSD), Michael F. Vansco (Penn), and Marisa C. Kozlowski (Penn) for helpful conversations.

#### References

- 1. D. Johnson; G. Marston, The gas-phase ozonolysis of unsaturated volatile organic compounds in the troposphere. *Chem. Soc. Rev.* **2008**, *37*, 699-716.
- 2. K. Sindelarova; C. Granier; I. Bouarar; A. Guenther; S. Tilmes; T. Stavrakou; J. F. Müller; U. Kuhn; P. Stefani; W. Knorr, Global data set of biogenic VOC emissions calculated by the MEGAN model over the last 30 years. *Atmos. Chem. Phys.* **2014**, *14*, 9317-9341.
- 3. R. M. Harrison; J. Yin; R. M. Tilling; X. Cai; P. W. Seakins; J. R. Hopkins; D. L. Lansley; A. C. Lewis; M. C. Hunter; D. E. Heard, et al., Measurement and modelling of air pollution and atmospheric chemistry in the U.K. West Midlands conurbation: Overview of the PUMA consortium project. *Sci. Total Environ.* **2006**, *360*, 5-25.
- 4. K. M. Emmerson; N. Carslaw; D. C. Carslaw; J. D. Lee; G. McFiggans; W. J. Bloss; T. Gravestock; D. E. Heard; J. Hopkins; T. Ingham, et al., Free radical modelling studies during the UK TORCH campaign in summer 2003. *Atmos. Chem. Phys.* **2007**, *7*, 167-181.
- 5. J. H. Kroll; S. R. Sahay; J. G. Anderson; K. L. Demerjian; N. M. Donahue, Mechanism of  $HO_x$  formation in the gas-phase ozone-alkene reaction. 2. Prompt versus thermal dissociation of carbonyl oxides to form OH. *J. Phys. Chem. A* **2001**, *105*, 4446-4457.
- 6. N. M. Donahue; G. T. Drozd; S. A. Epstein; A. A. Presto; J. H. Kroll, Adventures in ozoneland: Down the rabbit-hole. *Phys. Chem. Chem. Phys.* **2011**, *13*, 10848-10857.
- 7. G. T. Drozd; T. Kurtén; N. M. Donahue; M. I. Lester, Unimolecular decay of the dimethyl-substituted Criegee intermediate in alkene ozonolysis: Decay time scales and the importance of tunneling. *J. Phys. Chem. A* **2017**, *121*, 6036-6045.
- 8. A. Novelli; L. Vereecken; J. Lelieveld; H. Harder, Direct observation of OH formation from stabilised Criegee intermediates. *Phys. Chem. Chem. Phys.* **2014**, *16*, 19941-19951.
- 9. J. H. Kroll; T. F. Hanisco; N. M. Donahue; K. L. Demerjian; J. G. Anderson, Accurate, direct measurements of OH yields from gas-phase ozone-alkene reactions using an in situ LIF instrument. *Geophys. Res. Lett.* **2001**, *28*, 3863-3866.
- 10. L. Vereecken; A. Novelli; D. Taraborrelli, Unimolecular decay strongly limits the atmospheric impact of Criegee intermediates. *Phys. Chem. Chem. Phys.* **2017**, *19*, 31599-31612.
- 11. Y. Fang; V. P. Barber; S. J. Klippenstein; A. B. McCoy; M. I. Lester, Tunneling effects in the unimolecular decay of (CH<sub>3</sub>)<sub>2</sub>COO Criegee intermediates to OH radical products. *J. Chem. Phys.* **2017**, *146*, 134307.
- 12. Y. Fang; F. Liu; V. P. Barber; S. J. Klippenstein; A. B. McCoy; M. I. Lester, Deep tunneling in the unimolecular decay of CH<sub>3</sub>CHOO Criegee intermediates to OH radical products. *J. Chem. Phys.* **2016**, *145*, 234308.
- 13. Y. Fang; F. Liu; V. P. Barber; S. J. Klippenstein; A. B. McCoy; M. I. Lester, Communication: Real time observation of unimolecular decay of Criegee intermediates to OH radical products. *J. Chem. Phys.* **2016**, *144*, 061102.
- 14. L. Vereecken; J. S. Francisco, Theoretical studies of atmospheric reaction mechanisms in the troposphere. *Chem. Soc. Rev.* **2012**, *41*, 6259-6293.
- 15. F. Liu; J. M. Beames; M. I. Lester, Direct production of OH radicals upon CH overtone activation of (CH<sub>3</sub>)<sub>2</sub>COO Criegee intermediates. *J. Chem. Phys.* **2014**, *141*, 234312.
- 16. F. Liu; J. M. Beames; A. S. Petit; A. B. McCoy; M. I. Lester, Infrared-driven unimolecular reaction of CH<sub>3</sub>CHOO Criegee intermediates to OH radical products. *Science* **2014**, *345*, 1596-1598.

- 17. Y. Fang; F. Liu; S. J. Klippenstein; M. I. Lester, Direct observation of unimolecular decay of CH<sub>3</sub>CH<sub>2</sub>CHOO Criegee intermediates to OH radical products. *J. Chem. Phys.* **2016**, *145*, 044312.
- 18. V. P. Barber; S. Pandit; V. J. Esposito; A. B. McCoy; M. I. Lester, CH stretch activation of CH₃CHOO: Deep tunneling to hydroxyl radical products. *J. Phys. Chem. A* **2019**, *123*, 2559-2569.
- 19. R. L. Mauldin III; T. Berndt; M. Sipilä; P. Paasonen; T. Petäjä; S. Kim; T. Kurtén; F. Stratmann; V. M. Kerminen; M. Kulmala, A new atmospherically relevant oxidant of sulphur dioxide. *Nature* **2012**, *488*, 193.
- 20. J. P. Hakala; N. M. Donahue, Pressure-dependent Criegee intermediate stabilization from alkene ozonolysis. *J. Phys. Chem. A* **2016**, *120*, 2173-2178.
- 21. W. Chao; J.-T. Hsieh; C.-H. Chang; J. J.-M. Lin, Direct kinetic measurement of the reaction of the simplest Criegee intermediate with water vapor. *Science* **2015**, *347*, 751-754.
- 22. H.-L. Huang; W. Chao; J. J.-M. Lin, Kinetics of a Criegee intermediate that would survive high humidity and may oxidize atmospheric SO<sub>2</sub>. *Proc. Natl. Acad. Sci.* **2015**, *112*, 10857-10862.
- 23. L.-C. Lin; H.-T. Chang; C.-H. Chang; W. Chao; M. C. Smith; C.-H. Chang; J. Jr-Min Lin; K. Takahashi, Competition between H<sub>2</sub>O and (H<sub>2</sub>O)<sub>2</sub> reactions with CH<sub>2</sub>OO/CH<sub>3</sub>CHOO. *Phys. Chem. Phys.* **2016**, *18*, 4557-4568.
- 24. T. R. Lewis; M. A. Blitz; D. E. Heard; P. W. Seakins, Direct evidence for a substantive reaction between the Criegee intermediate, CH<sub>2</sub>OO, and the water vapour dimer. *Phys. Chem. Phys.* **2015**, *17*, 4859-4863.
- 25. O. Welz; J. D. Savee; D. L. Osborn; S. S. Vasu; C. J. Percival; D. E. Shallcross; C. A. Taatjes, Direct kinetic measurements of Criegee intermediate (CH<sub>2</sub>OO) formed by reaction of CH<sub>2</sub>I with O<sub>2</sub>. *Science* **2012**, *335*, 204-207.
- 26. C. A. Taatjes; O. Welz; A. J. Eskola; J. D. Savee; A. M. Scheer; D. E. Shallcross; B. Rotavera; E. P. F. Lee; J. M. Dyke; D. K. W. Mok, et al., Direct measurements of conformer-dependent reactivity of the Criegee intermediate CH<sub>3</sub>CHOO. *Science* **2013**, *340*, 177-180.
- 27. L. Vereecken; H. M. T. Nguyen, Theoretical study of the reaction of carbonyl oxide with nitrogen dioxide:  $CH_2OO + NO_2$ . *Int. J. Chem. Kinet.* **2017**, *49*, 752-760.
- 28. R. L. Caravan; M. A. H. Khan; B. Rotavera; E. Papajak; I. O. Antonov; M.-W. Chen; K. Au; W. Chao; D. L. Osborn; J. J.-M. Lin, et al., Products of Criegee intermediate reactions with NO<sub>2</sub>: Experimental measurements and tropospheric implications. *Faraday Discuss.* **2017**, *200*, 313-330.
- 29. B. Ouyang; M. W. McLeod; R. L. Jones; W. J. Bloss,  $NO_3$  radical production from the reaction between the Criegee intermediate  $CH_2OO$  and  $NO_2$ . *Phys. Chem. Chem. Phys.* **2013**, *15*, 17070-17075.
- 30. Y. Liu; K. D. Bayes; S. P. Sander, Measuring rate constants for reactions of the simplest Criegee intermediate (CH<sub>2</sub>OO) by monitoring the OH radical. *J. Phys. Chem. A* **2014**, *118*, 741-747.
- 31. L. Sheps, Absolute ultraviolet absorption spectrum of a Criegee intermediate CH<sub>2</sub>OO. *J. Phys. Chem. Lett.* **2013**, *4*, 4201-4205.
- 32. J. H. Kroll; J. H. Seinfeld, Chemistry of secondary organic aerosol: Formation and evolution of low-volatility organics in the atmosphere. *Atmos. Environ.* **2008**, *42*, 3593-3624.

- 33. T. B. Nguyen; G. S. Tyndall; J. D. Crounse; A. P. Teng; K. H. Bates; R. H. Schwantes; M. M. Coggon; L. Zhang; P. Feiner; D. O. Milller, et al., Atmospheric fates of Criegee intermediates in the ozonolysis of isoprene. *Phys. Chem. Chem. Phys.* **2016**, *18*, 10241-10254.
- 34. R. Gutbrod; E. Kraka; R. N. Schindler; D. Cremer, Kinetic and theoretical investigation of the gas-phase ozonolysis of isoprene: Carbonyl oxides as an important source for OH radicals in the atmosphere. *J. Am. Chem. Soc.* **1997**, *119*, 7330-7342.
- 35. R. Atkinson; S. M. Aschmann; J. Arey; B. Shorees, Formation of OH radicals in the gas phase reactions of O<sub>3</sub> with a series of terpenes. *J. Geophys. Res.* **1992,** *97,* 6065-6073.
- 36. S. E. Paulson; R. C. Flagan; J. H. Seinfeld, Atmospheric photooxidation of isoprene part II: The ozone-isoprene reaction. *Int. J. Chem. Kinet.* **1992,** *24*, 103-125.
- 37. K. T. Kuwata; L. C. Valin; A. D. Converse, Quantum chemical and master equation studies of the methyl vinyl carbonyl oxides formed in isoprene ozonolysis. *J. Phys. Chem. A* **2005**, *109*, 10710-10725.
- 38. K. T. Kuwata; L. C. Valin, Quantum chemical and RRKM/master equation studies of isoprene ozonolysis: Methacrolein and methacrolein oxide. *Chem. Phys. Lett.* **2008**, *451*, 186-191.
- 39. D. Zhang; R. Zhang, Mechanism of OH formation from ozonolysis of isoprene: A quantum-chemical study. *J. Am. Chem. Soc.* **2002**, *124*, 2692-2703.
- 40. M. Nakajima; Y. Endo, Communication: Spectroscopic characterization of an alkyl substituted Criegee intermediate *syn*-CH<sub>3</sub>CHOO through pure rotational transitions. *J. Chem. Phys.* **2014**, *140*, 011101.
- 41. C. Cabezas; J.-C. Guillemin; Y. Endo, Conformational analysis of ethyl-substituted Criegee intermediate by FTMW spectroscopy. *J. Chem. Phys.* **2016**, *145*, 224314.
- 42. C. Cabezas; J.-C. Guillemin; Y. Endo, Probing the conformational behavior of the doubly substituted methyl-ethyl Criegee intermediate by FTMW spectroscopy. *J. Chem. Phys.* **2017**, *146*, 174304.
- 43. M. Nakajima; Y. Endo, Communication: Determination of the molecular structure of the simplest Criegee intermediate CH<sub>2</sub>OO. *J. Chem. Phys.* **2013**, *139*, 101103.
- 44. M. Nakajima; Q. Yue; Y. Endo, Fourier-transform microwave spectroscopy of an alkyl substituted Criegee intermediate *anti*-CH<sub>3</sub>CHOO. *J. Mol. Spectrosc.* **2015**, *310*, 109-112.
- 45. M. Nakajima; Y. Endo, Fourier-transform microwave spectroscopy of dimethylsubstituted Criegee intermediate (CH<sub>3</sub>)<sub>2</sub>COO. *J. Chem. Phys.* **2016**, *145*, 244307.
- 46. J. M. Beames; F. Liu; L. Lu; M. I. Lester, Ultraviolet spectrum and photochemistry of the simplest Criegee intermediate  $CH_2OO$ . J. Am. Chem. Soc. **2012**, 134, 20045-20048.
- 47. J. M. Beames; F. Liu; L. Lu; M. I. Lester, UV spectroscopic characterization of an alkyl substituted Criegee intermediate CH<sub>3</sub>CHOO. *J. Chem. Phys.* **2013**, *138*, 244307.
- 48. L. Sheps; A. M. Scully; K. Au, UV absorption probing of the conformer-dependent reactivity of a Criegee intermediate CH<sub>3</sub>CHOO. *Phys. Chem. Chem. Phys.* **2014**, *16*, 26701-26706.
- 49. Y.-P. Chang; C.-H. Chang; K. Takahashi; J. J.-M. Lin, Absolute UV absorption cross sections of dimethyl substituted Criegee intermediate (CH<sub>3</sub>)<sub>2</sub>COO. *Chem. Phys. Lett.* **2016**, *653*, 155-160.
- 50. F. Liu; J. M. Beames; A. M. Green; M. I. Lester, UV spectroscopic characterization of dimethyl- and ethyl-substituted carbonyl oxides. *J. Phys. Chem. A* **2014**, *118*, 2298-2306.
- 51. V. P. Barber; A. S. Hansen; Y. Georgievskii; S. J. Klippenstein; M. I. Lester, Experimental and theoretical studies of the double-substituted methyl ethyl Criegee

- intermediate: Infrared action spectroscopy and unimolecular decay to OH radical products. *J. Chem. Phys.* **2020**, *152*, 094301.
- 52. V. P. Barber; S. Pandit; A. M. Green; N. Trongsiriwat; P. J. Walsh; S. J. Klippenstein; M. I. Lester, Four-carbon criegee intermediate from isoprene ozonolysis: Methyl vinyl ketone oxide synthesis, infrared spectrum, and OH production. *J. Am. Chem. Soc.* **2018**, *140*, 10866-10880.
- 53. M. F. Vansco; B. Marchetti; M. I. Lester, Electronic spectroscopy of methyl vinyl ketone oxide: A four-carbon unsaturated Criegee intermediate from isoprene ozonolysis. *J. Chem. Phys.* **2018**, *149*, 244309.
- 54. M. F. Vansco; B. Marchetti; N. Trongsiriwat; G. Wang; T. Bhagde; P. J. Walsh; S. J. Klippenstein; M. I. Lester, Synthesis, electronic spectroscopy and photochemistry of methacrolein oxide: A four carbon unsaturated Criegee intermediate from isoprene ozonolysis. *J. Am. Chem. Soc.* **2019**, *141*, 15058-15069.
- R. L. Caravan; M. F. Vansco; K. Au; M. Anwar H. Khan; Y.-L. Lie; F. A. F. Winiberg; K. Zuraskia; Y.-H. Line; W. Chao; N. Trongsiriwat, et al., Direct kinetic measurements and theoretical predictions of an isoprene-derived Criegee intermediate. *Proc. Natl. Acad. Sci.* **2020**, *117*, 9733-9740.
- 56. M. F. Vansco; R. L. Caravan; K. Zuraski; F. A. F. Winiberg; K. Au; N. Trongsiriwat; P. J. Walsh; D. L. Osborn; C. J. Percival; C. A. Taatjes, et al., Experimental evidence of dioxole unimolecular decay pathway for isoprene-derived Criegee intermediates. *J. Phys. Chem. A* **2020**, *124*, 3542-3554.
- 57. A. M. Green; V. P. Barber; Y. Fang; S. J. Klippenstein; M. I. Lester, Selective deuteration illuminates the importance of tunneling in the unimolecular decay of Criegee intermediates to hydroxyl radical products. *Proc. Natl. Acad. Sci.* **2017**, *114*, 12372-12377.
- 58. K. T. Kuwata; M. R. Hermes; M. J. Carlson; C. K. Zogg, Computational Studies of the Isomerization and Hydration Reactions of Acetaldehyde Oxide and Methyl Vinyl Carbonyl Oxide. *J. Phys. Chem. A* **2010**, *114*, 9192-9204.
- 59. L. Vereecken; H. Harder; A. Novelli, The reaction of Criegee intermediates with NO, RO<sub>2</sub>, and SO<sub>2</sub>, and their fate in the atmosphere. *Phys. Chem. Chem. Phys.* **2012**, *14*, 14682-14695.
- 60. M. J. Frisch; G. W. Trucks; H. B. Schlegel; G. E. Scuseria; M. A. Robb; J. R. Cheeseman; G. Scalmani; V. Barone; G. A. Petersson; H. Nakatsuji, et al., Gaussian 16 Rev. A.03. **2016**, Gaussian, Inc., Wallingford CT.
- 61. S. Grimme; S. Ehrlich; L. Goerigk, Effect of the damping function in dispersion corrected density functional theory. *J. Comp. Chem.* **2011**, *32*, 1456-1465.
- 62. L. Goerigk; S. Grimme, Efficient and accurate double-hybrid-meta-GGA density functionals-evaluation with the extended GMTKN30 database for general main group thermochemistry, kinetics, and noncovalent interactions. *J. Chem. Theory Comput.* **2011,** *7*, 291-309.
- 63. J. Towns; T. Cockerill; M. Dahan; I. Foster; K. Gaither; A. Grimshaw; V. Hazlewood; S. Lathrop; D. Lifka; G. D. Peterson, et al., XSEDE: Accelerating scientific discovery. *Comput. Sci. Eng.* **2014**, *16*, 62-74.
- 64. T. Baer; W. L. Hase, *Unimolecular reaction dynamics theory and experiments*. Oxford University Press: New York, 1996.
- 65. J. R. Barker, T. L. Nguyen, J. F. Stanton, C. Aieta, M. Ceotto, F. Gabas, T. J. D. Kumar, C. G. L. Li, L. Lohr, A. Maranzana, N. F. Ortiz, J. M. Preses, J. M. Simmie, J. A. Sonk, and P. J.

- Stimac; MultiWell-2019 Software Suite; J. R. Barker, University of Michigan, Ann Arbor, Michigan, USA, (2019); <a href="http://clasp-research.engin.umich.edu/multiwell/">http://clasp-research.engin.umich.edu/multiwell/</a>.
- 66. D. J. Nesbitt; R. W. Field, Vibrational energy flow in highly excited molecules: Role of intramolecular vibrational redistribution. *J. Phys. Chem.* **1996**, *100*, 12735-12756.
- 67. M.-C. Yoon; Y. S. Choi; S. K. Kim, Photodissociation dynamics of acetylacetone: The OH product state distribution. *J. Chem. Phys.* **1999**, *110*, 11850-11855.
- 68. M.-C. Yoon; Y. S. Choi; S. K. Kim, The OH production from the  $\pi$ - $\pi$ \* transition of acetylacetone. *Chem. Phys. Lett.* **1999**, *300*, 207-212.
- 69. I. Antonov; K. Voronova; M.-W. Chen; B. Sztáray; P. Hemberger; A. Bodi; D. L. Osborn; L. Sheps, To boldly look where no one has looked before: Identifying the primary photoproducts of acetylacetone. *J. Phys. Chem. A* **2019**, *123*, 5472-5490.

## TOC Graphic

